Multimed Tools Appl (2016) 75:7589–7604
DOI 10.1007/s11042-015-2682-6

EMCCD color correction based on spectral sensitivity analysis

Jongin Son[1] · **Minsung Kang**[1] · **Dongbo Min**[1,2] · **Kwanghoon Sohn**[1]

Received: 28 September 2014 / Revised: 11 March 2015 / Accepted: 6 May 2015 /
Published online: 26 May 2015

Abstract The sensor response function of a color camera is very essential to understand an overall camera imaging pipeline and to process captured images. It is also true when we characterize underlying imaging behaviors of the electron multiplying charge coupled device (EMCCD) camera, which was recently proposed to acquire color images in low-light-level conditions. Unlike existing CCD cameras, the EMCCD camera contains partially uni-modal spectral sensitivity functions (SSFs), some of which consists of two base (bi-modal) functions, thus often leading to a serious color distortion in existing characterization techniques. To address this problem, we propose a novel method that corrects output colors of the EMCCD camera by analyzing its partially uni-modal characteristics. Specifically, our goal is to correct such color distortion by adjusting bi-modal SSFs to be uni-modal. We remove the secondary region of bi-modal channels using a pre-calculated spectral sensitivity of the EMCCD camera. Experimental results demonstrate that the proposed method reduces the color distortion as well as enlarges a color gamut, which is crucial to color reproduction.

Keywords Color correction · EMCCD · Spectral sensitivity

✉ Kwanghoon Sohn
khsohn@yonsei.ac.kr

Jongin Son
go3son@yonsei.ac.kr

Minsung Kang
mskang83@gmail.com

Dongbo Min
dbmin@cnu.ac.kr

[1] Department of Electrical and Electronic Engineering, Yonsei University, Seoul 120-749, Korea

[2] Department of Computer Science and Engineering, Chungnam National University, Daejeon 305-764, Korea

1 Introduction

Several types of image sensors such as the charge coupled device (CCD) and the complementary metal-oxide-semiconductor (CMOS) have been widely used for an image acquisition. For a variety of reasons, acquiring high-quality images in a low-light-level condition has also become increasingly crucial, especially in surveillance applications [8]. However, such imaging sensors have certain limitations in capturing images in a low-light-level condition. An infrared camera is generally used for low-light-level imaging, but it can capture a single channel image only. Recently, there have been some remarkable hardware advances in the low-light imaging, e.g., an intensified CCD (ICCD) [9], electron-bombarded CCD (EBCCD) [13], and electron multiplying CCD (EMCCD) [3]. In particular, the EMCCD performs very well in extremely low-light-level conditions, in which either intensified or slow-scan sensors were previously used [11]. The EMCCD technology was first introduced to the imaging community in 2002 by the Andor Technology, a public limited company [3]. Afterward, the company has organized a forum for discussing and sharing ideas for the EMCCD technology (http://www.EMCCD.com).

In principle, the EMCCD produces a gain through impact ionization by adding multiplication or gain registers to an output register. Its advantage over the CCD camera is that the gain is applied prior to a readout, thus minimizing deleterious effects of the readout noise in low-light-level conditions [9, 12]. The EMCCD research has been becoming popular among the imaging community [2, 3, 11, 12, 17, 18, 21]. Kriesel and Gat [17, 18] focused on applying the EMCCD camera to a night vision system for improving image quality. Color imaging in low-light-level condition can benefit from the EMCCD camera, e.g., by applying existing image processing algorithms, which are usually available only in sufficient lighting conditions, to the EMCCD images captured in low-light-level condition.

In order to make use of an EMCCD camera in imaging applications, we should characterize the recording device and analyze images captured in the low-lighting condition. Specifically, the device characterization techniques are applied to minimize the impact of device limitations and differences and to preserve original color information during an image transfer between devices [24]. Typically, the spectral characteristics of the sensor are not available from manufacturers, so a user should characterize the device. There are numerous researches for the device characterization [1, 4, 7, 10, 14, 22, 25]. Recently, Kang et al. adopted these spectral sensitivity estimation approaches to the EMCCD camera [16], and found that its spectral sensitivity is partially bi-modal, unlike that of conventional CCD cameras. They also showed that such a partially bi-modal sensitivity function causes a serious color distortion. Figure 1 shows the ratio of RGB colors of gray patches. Two EMCCD images were captured under 6 and 100 lx lighting conditions as a low-light-level image and a reference image, respectively. The reference image is assumed to produce very precise color images, since the EMCCD camera is converted into the CCD mode in the sufficient lighting condition. As shown in Fig. 1, the RGB ratio of indexed gray patches is almost constant in the reference image, while the ratio in the low-light-level image varies according to the gray level. Especially, an intensity of the blue channel in the low-light-level image is very different from those of other channels, which is the major cause of the color distortion problem. Correcting such distortion caused by the partially uni-modal spectral sensitivity function (SSF), however, has not been explored so far.

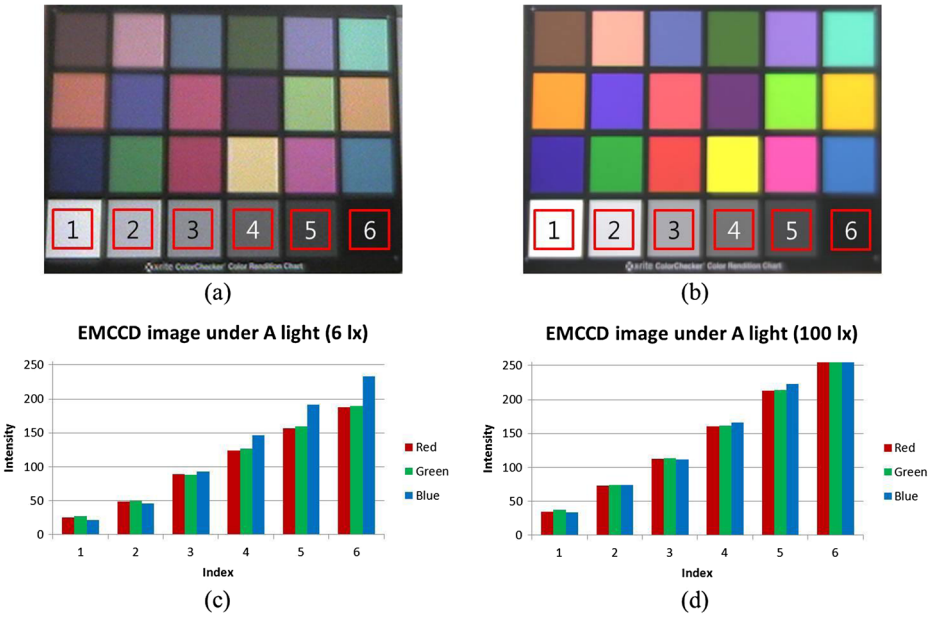

Fig. 1 Ratio of RGB colors in *gray* patches captured by EMCCD camera: Captured image under A light (**a**) 6 lx and (**b**) 100 lx. RGB plots of the indexed patches captured under (**c**) 6 lx and (**d**) 100 lx

In this paper, we propose a color correction algorithm that addresses the color distortion problem of the EMCCD camera. The main contributions of this paper can be summarized as follows:

- We define characteristics of EMCCD camera by analyzing its partially uni-modal and propose correction method.
- We remove the secondary region of bi-modal channels using a pre-calculated spectral sensitivity of the EMCCD camera and demonstrate that the proposed method reduces the color distortion

The remainder of this paper is organized as follows: Section 2 introduces a basic background on the EMCCD camera and describes its general camera model in detail. The color correction method is then proposed in Section 3. Section 4 presents experimental setting and results. Finally, Section 5 concludes our work and discusses future works.

2 Background

2.1 Electron multiplying charge coupled device

The operation principle of the EMCCD was first introduced by Jerram et al. [11] as a low-light-level CCD (LLLCCD). It has been known that the ultimate sensitivity of a conventional CCD is limited by the noise incurred by a charge-to-voltage conversion process. Since the readout noise increases with a pixel rate, several applications requiring a high sensitivity

should employ a slow readout in order to minimize the noise. In contrast, the sensitivity function of the EMCCD camera is not limited by the readout noise of the output amplifier, even when operated at high readout speeds. Figure 2 shows the structure of the EMCCD where a solid state electron multiplying (EM) register is inserted between the readout register and the on-chip charge in the voltage conversion circuitry. The other parts (such as store and readout registers) are the same as those of the conventional design.

Figure 3 shows color images obtained from the CCD camera and the EMCCD camera under varying lighting conditions. The EMCCD camera SHC-750 (http://www.samsungcctv.co.kr) with 658×496 resolution was used. The EMCCD camera provides color images with relatively good quality even in the extremely low-lighting condition (e.g., 0.3 lx) where the images of the CCD camera contain no valid color data. However, as mentioned earlier, there exist color distortions that should be corrected, e.g., in the blue channel as shown in Fig. 1.

2.2 The camera model

In this section, we discuss a general camera model commonly used in the EMCCD camera as well as the CCD camera. All camera control parameters (e.g., aperture and focal length) are assumed to be fixed. The image acquisition process can be mathematically modeled with a light, object, and sensor. Let $E(p,\lambda)$ and $S(p,\lambda)$ denote a spectral power distribution of an incident light and a surface reflectance of an object for a wavelength λ, respectively. The spectral power distribution of a signal reflected from the object can be defined as $L(p,\lambda)=E(p,\lambda)S(p,\lambda)$. Also, let $I_k(p)$ denote an output (intensity) of a color band $k\in\{R,G,B\}$ at a pixel $p=(x,y)$. The image acquisition model can then be formulated as [1]

$$I_k(p) = \int_\omega E(p,\lambda)S(p,\lambda)Q_k(\lambda)d\lambda = \int_\omega L(p,\lambda)Q_k(\lambda)d\lambda \tag{1}$$

where $Q_k(\lambda)$ represents the SSF of the k^{th} channel in a camera sensor. The integration is performed over a visible spectrum (i.e., 380~730 nm). In practice, the continuous

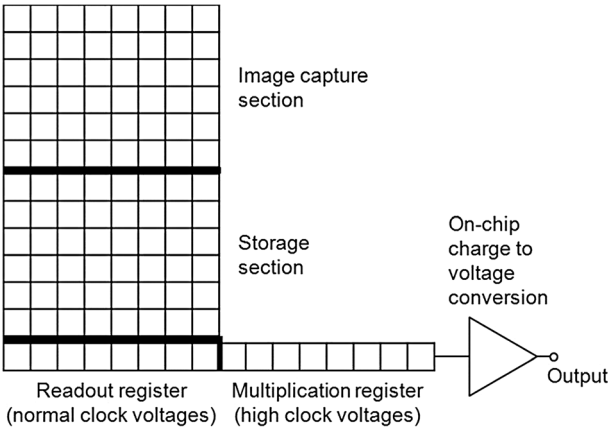

Fig. 2 CCD of Electron Multiplying Register (http://www.EMCCD.com)

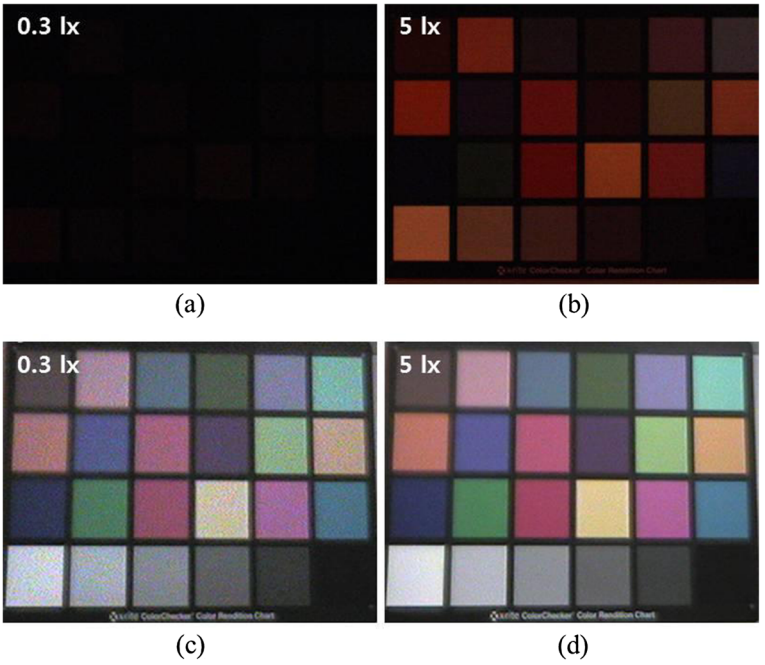

Fig. 3 Visual comparison of color images under low lighting conditions: **a** CCD camera under 0.3 lx, **b** CCD camera under 5 lx, **c** EMCCD camera under 0.3 lx and **d** EMCCD camera under 5 lx

wavelength λ is sampled at regular intervals using $\Delta\lambda$ inside the given visible spectrum ω. We define a set of regularly quantized wavelength values over the visible spectrum as $\omega_I=\{\lambda_m|\lambda_m=m\Delta\lambda,\ [\lambda_{min}/\Delta\lambda]\leq m\Delta\lambda\leq[\lambda_{max}/\Delta\lambda],m:integer\}$, where λ_{min} and $\lambda_{\max}$ represent the minimum and maximum wavelength of the visible spectrum. A discrete form of (1) is then written as

$$I_k(p)=\sum_{\lambda_m\in\omega_I} L(p,\lambda)Q_k(\lambda_m)\Delta\lambda,\ (k=R,G,B) \tag{2}$$

To estimate the SSF $Q_k(\lambda)$, we first measure the spectral data $L(p,\lambda)$ and the corresponding intensity I_k using a color chart. $Q_k(\lambda)$ is then estimated using the regularized least-squares regression and the regularization with a Fourier smoothing constraint [1, 7].

3 Color correction using SSF

As explained earlier, the SSF of the EMCCD is partially bi-modal [16]. Figure 4 shows the example of SSFs measured from the EMCCD camera. Especially, the green and blue channels have bi-modal SSF consisting of two base functions, while that of the red channel is an uni-modal base function. To reflect these characteristics, we divide the wavelength range ω_l into two non-overlapping ω_{l1} and ω_{l2}, i.e., $\omega_{l1}\cup\omega_{l2}=\omega$ and $\omega_{l1}\cap\omega_{l2}=\varnothing$ for $l=G,B$. For instance, in Fig. 4, ω_{G2} and ω_{B2} are 610~680 nm and 560~710 nm. It should be noted that the wavelength

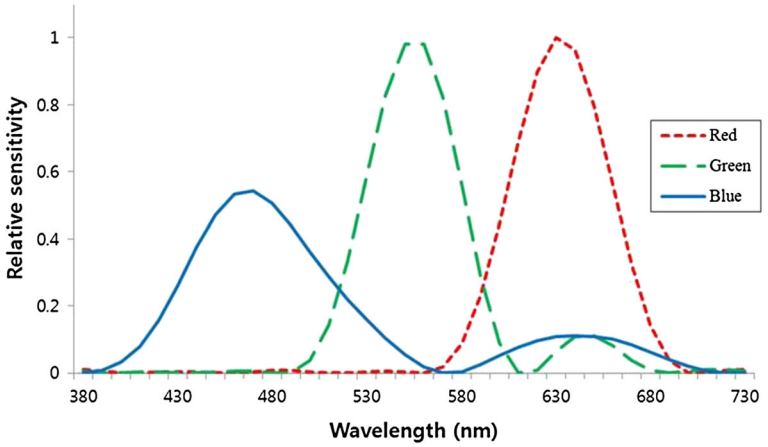

Fig. 4 Spectral sensitivity of the EMCCD camera [16]

ranges may vary according to the EMCCD camera used, but these can be pre-calculated in the calibration stage.

$$\begin{aligned} I_R(p) &= \sum_{\omega_I} L(p,\lambda) Q_R(\lambda) \Delta\lambda \\ I_G(p) &= I_{G1}(p) + I_{G2}(p) \\ &= \sum_{\omega_{G1}} L(p,\lambda) Q_G(\lambda) \Delta\lambda + \sum_{\omega_{G2}} L(p,\lambda) Q_G(\lambda) \Delta\lambda \\ I_B(p) &= I_{B1}(p) + I_{B2}(p) \\ &= \sum_{\omega_{B1}} L(p,\lambda) Q_B(\lambda) \Delta\lambda + \sum_{\omega_{B2}} L(p,\lambda) Q_B(\lambda) \Delta\lambda, \end{aligned} \tag{3}$$

where I_{G2} and I_{B2} represent intensity values generated by the secondary SSFs, which should be removed for color correction. Our goal is to estimate I_{G1} and I_{B1} when color intensity values I_k and their corresponding SSFs Q_k are given for each color channel $k \in \{R,G,B\}$. Note that Q_k is pre-calculated in the sensor calibration stage [1, 7, 16]. Interestingly, it was observed that the uni-modal SSF of the R channel shares the similar wavelength band with the secondary SSFs of G and B channels. Using this observation, we define the intensity value incurred by the secondary SSF as follows:

$$I_{l2}(p) = \alpha_l I_R(p) = \alpha_l \sum_{\omega_I} L(p,\lambda) Q_R(\lambda) \Delta\lambda, (l = G,B) \tag{4}$$

where $\alpha_l (l=G,B)$ represents a correction parameter with a range of $0 \leq \alpha_l \ll 1$. More specifically, it enables estimating the intensity values incurred by the secondary SSF without using $L(p,\lambda)$. Instead, $I_{l2}(p)$ is directly estimated from $I_R(p)$ with the correction parameter α_l. Figure 3 also shows that the bandwidth of the uni-modal SSF of the R channel is almost overlapped with that of the secondary SSFs of the G and B channels.

In this section, we explain the estimation of parameters for color correction using SSF. We proposed two color correction methods. Section 3.1 uses the basic Dirac delta function with

the secondary region of B channel. Section 3.2 uses the improved Dirac delta function and removes the secondary region of Bchannel for accurate color corrections.

3.1 Color correction using Dirac delta function

Now, we estimate the correction parameter α using only Dirac Delta Function assumption. Similar to existing works [5, 6], we assume the SSF of the R channel to be approximated with a Dirac delta function $Q_R(\lambda)=q_R\delta(\lambda-\lambda_R)$ where λ_R and q_R represent a peak point of the SSF and a relative sensitivity value, respectively. Then, $I_R(p)$ of (3) becomes

$$I_R(p) = \sum_{\omega_I} L(p,\lambda)\delta(\lambda-\lambda_R)\Delta\lambda = L(p,\lambda_R)q_R, \tag{5}$$

Hereafter, we assume $\Delta\lambda=1$ for simplicity. Note that this assumption does not affect corrected results. In contrast, the SSFs of the G and B channels are bi-modal, and thus they are defined as $Q_l(\lambda)=q_{l1}\delta(\lambda-\lambda_{l1})+q_{l2}\delta(\lambda-\lambda_{l2})$, $(l=G,B)$ comprising two Dirac delta functions. λ_{l1} and λ_{l2} represents the primary and secondary peak points of the SSF, and q_{l1} and q_{l2} are the relative sensitivity values at two peak points. Here $\lambda_{l1}\in\omega_{l1}$ and $\lambda_{l2}\in\omega_{l2}$. $I_l(p)$ $(l=G,B)$ of (3) is then written as

$$\begin{aligned} I_l(p) &= I_{l1}(p) + I_{l2}(p) \\ &= \sum_{\omega_{l1}} L(p,\lambda)q_{l1}\delta(\lambda-\lambda_{l1}) + \sum_{\omega_{l2}} L(p,\lambda)q_{l2}\delta(\lambda-\lambda_{l2}) \\ &= L(p,\lambda_{l1})q_{l1} + L(p,\lambda_{l2})q_{l2}. \end{aligned} \tag{6}$$

By substituting (5) into (4),

$$I_{l2}(p) = \alpha_l L(p,\lambda_R)q_R. \tag{7}$$

We can induce the following equations by substituting (7) into (6):

$$\begin{cases} I_R(p) = L(p,\lambda_R)q_R I_l(p) = I_{l1}(p) + I_{l2}(p) \\ \qquad = L(p,\lambda_{l1})q_{l1} + \alpha_l L(p,\lambda_R)q_R, \ (l=G,B), \end{cases} \tag{8}$$

where the correction parameter α_l is derived as follows:

$$I_{l2}(p) = L(p,\lambda_{l2})q_{l2}. \tag{9}$$

By substituting (7) into (9),

$$L(p,\lambda_{l2})q_{l2} = \alpha_l L(p,\lambda_R)q_R, \tag{10}$$

$$\alpha_l = \frac{L(p,\lambda_{l2})\,q_{l2}}{L(p,\lambda_R)\,q_R}, \tag{11}$$

With the observation $\omega_R\approx\omega_{l2}$ described in (4), that is $L(p,\lambda_{l2})\approx L(p,\lambda_R)$. Finally the correction parameter α_l becomes,

$$\alpha_l = q_{l2}/q_R. \tag{12}$$

With the estimated α_l $(l=G,B)$, intensity values I_{l1} obtained by the color corrected uni-modal SSF can be easily calculated as follows:

$$I_{l1}(p) = I_l(p) - I_{l2}(p) = I_l(p) - \alpha_l I_R(p). \tag{13}$$

3.2 Color correction using L2-norm Regularization

We have approximated the SSF $Q_k(\lambda)$ using a set of the Dirac delta functions with peak points (λ_R, λ_{l1}, and λ_{l2}) and relative sensitivity values (q_R, q_{l1}, and q_{l2}). This simple approximation, however, does not represent the region of $Q_k(\lambda)$ accurately. For instance, there are two normal distributed curves which have the same intensity at a peak point yet with different standard deviations (σ). In this case, with the Dirac delta function assumption, two curves have the same sensitivity value (q_l) at peak points (i.e., $\alpha_G=\alpha_B$). We use optimization technique to estimate the correction parameter α_l instead of the Dirac delta assumption. With the observation $\omega_R \approx \omega_{l2}$, Eq. (4) can be described as follows:

$$I_{l2}(p) - \alpha_l I_R(p) = 0, (l = G, B), \tag{14}$$

$$\sum_{\omega_{l2}} L(p,\lambda) Q_{l2}(\lambda) \Delta\lambda - \alpha_l \sum_{\omega_R} L(p,\lambda) Q_R(\lambda) \Delta\lambda = 0. \tag{15}$$

With the observation $\omega_R \approx \omega_{l2}$,

$$\sum_{\omega_R} L(p,\lambda) \{\alpha_l Q_R(\lambda) - Q_{l2}(\lambda)\} = 0. \tag{16}$$

It is obvious that the reflected spectral power distribution $L(p,\lambda)$ is arbitrary positive real value ($L(p,\lambda) \in \mathbb{R}$, $L(p,\lambda) \geq 0$), and we assume that $L(p,\lambda)$ is slowly varying in narrow wavelength range such as ω_R. With these assumed premise, we can minimize the second term using least squares regularization method. The second term can be re-described as a least squares form and we can calculate the correction parameter α_l which minimize the second term:

$$\underset{\alpha_l > 0}{argmin} \|\alpha_\mathbf{l} \mathbf{Q_R} - \mathbf{Q_{l2}}\|_2^2 \tag{17}$$

In order to solve the least squares problem, we use the Tikonov regularization method. The regularization term is designed as follows:

$$\underset{\alpha_l > 0}{argmin} \left(\|\alpha_\mathbf{l} \mathbf{Q_R} - \mathbf{Q_{l2}}\|_2^2 + \lambda \|\alpha_\mathbf{l}\|_2^2 \right), \tag{18}$$

where λ is regularization parameter which controls the weight of the smoothness term. And its analytic solution becomes

$$\alpha_l = \left(\mathbf{Q_R}^\mathbf{T} \mathbf{Q_R} + \lambda \mathbf{I} \right)^{-1} \mathbf{Q_R}^T \mathbf{Q_{l2}}. \tag{19}$$

In order to confirm the effect of the proposed correction method, we re-estimate the SSF of the EMCCD after color correction [16]. Specifically, we perform the regularized least-squares regression with the SSF corrected intensity values ($I_R(p)$ and $I_{l1}(p)$, $l=G,B$). We found that the SSF was adjusted inaccurately in the secondary region of B channel as shown in Fig. 5a, when the Dirac delta function assumption in Section 3.1 was utilized. On the contrary, the method using the modified Dirac delta function in Section 3.2 precisely corrected the SSF to be unimodal as shown in Fig. 5b.

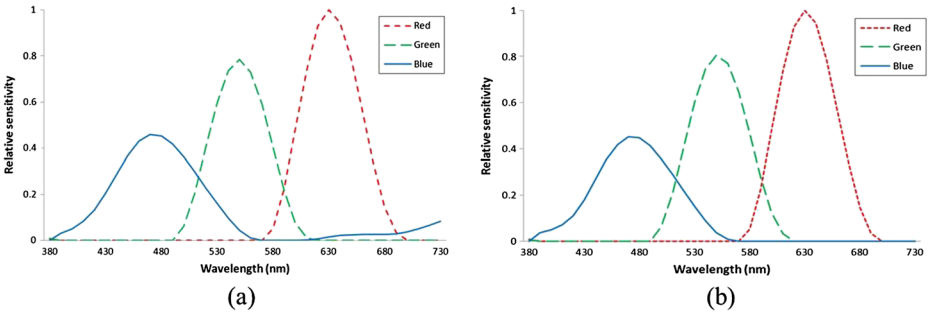

Fig. 5 SSF correction: **a** Dirac delta function and **b** L2-norm regularization

4 Experimental results

4.1 Experimental environment

An EMCCD camera 'Samsung SHC-750' (http://www.samsungcctv.co.kr) with an image size of 658×496 and lens 'Samsung MLZ-612AI' [16] were used for this study. The color chart employed is 'GretagMacbeth ColorChecker' (MCC) with 24 colors (http://xritephoto.com/). All the experiments were conducted in a darkroom with a lighting booth 'GretagMacbeth SpectraLight III' remodeled to control a lighting level. Low-light-level conditions used in the experiments are 6, 9, and 12 lx under standard D65 illumination. These lighting levels were empirically determined by measuring outdoor illumination conditions at night. We captured and averaged 20 consecutive images to suppress the EMCCD camera noise. Also, *RGB* color values corresponding to a central pixel of each color patch were measured to assure homogeneous regions, e.g., 3600 pixels for MCC (60 by 60 patches).

4.2 Performance evaluation

In order to calculate $\alpha_l (l=G,B)$ in (19), we use the EMCCD spectral sensitivity as shown in Fig. 4, which is from the previous work [16]. Using this data obtained from the calibration stage, the calculated constants α_l are $\alpha_G=0.0713, \alpha_B=0.1244$ with $\lambda=0.001$.

In order to demonstrate a quantitative improvement, we measured a root-mean-square error (RMSE) between an input color I and a reference color J which are extracted respectively from input image and reference image on CIEXYZ and CIELAB color spaces. The RMSE on the CIEXYZ and CIELAB color spaces are simply measured as follows:

$$\Delta E_{xyz} = \frac{1}{N}\sum_{n\in N}\left\{\sum_{m\in\{X,Y,Z\}}\left[\overline{I}_m(n)-\overline{J}_m(n)\right]^2\right\}^{1/2}, \tag{20}$$

$$\Delta E_{ab} = \frac{1}{N}\sum_{n\in N}\left\{\sum_{m\in\{L,a,b\}}\left[\overline{I}_m(n)-\overline{J}_m(n)\right]^2\right\}^{1/2}, \tag{21}$$

where N represents a set of colors extracted from a color chart, overline represents an average of pixels inside a patch. We evaluate our proposed color correction method by comparing input images (captured EMCCD image under low-light conditions) with reference image (captured EMCCD image under enough lighting conditions). The CIEDE2000 [23] and CAM02-UCS (uniform color space) [19] are also utilized for the performance evaluation considering a human visual system (HVS). The CIEDE2000 is general color distance metric. The simple CIEDE2000 color difference formula is as follows:

$$\Delta E_{00} = \frac{1}{N}\sum_{n\in N}\left\{\sum_{m\in\{L,C,H\}}\left[\frac{\overline{I}_m(n)-\overline{J}_m(n)}{k_m S_m}\right]^2 + (n)\right\}^{1/2}, \tag{22}$$

where $\overline{\Phi}(n) = R_T \frac{[\overline{I}_{C'}(n)-\overline{J}_{C'}(n)]}{k_C S_C} \frac{[\overline{I}_{H'}(n)-\overline{J}_{H'}(n)]}{k_H S_H}$. And L, C, and H are the CIELCH color space which is calculated from the CIELAB color space [23]. R_T is a hue rotation term. The parametric weighting factors k_L, k_C, and k_H are usually set to 1. S_L, S_C, and S_H represent the compensation parameters for lightness, chroma, and hue, respectively [23]. The CIECAM02 [4] is a color appearance model, which is known to be very effective in the HVS. This model presents an image in a realistic manner as if we would actually see it [15]. The CIECAM02 model uses five parameters: XYZ input, surrounding parameters including XYZ values of adapting black-and-white point, surrounding luminance information, and degree of discounting-the-illuminant. The CIECAM02 forward process yields outputs with 6-D color appearance: brightness (Q), lightness (J), colorfulness (M), chroma (C), saturation (S), and hue angle (h) [4]. Figure 6 shows the evaluation method using the CIECAM02 model.

Since two input images (original and corrected images) are captured by the EMCCD camera under low-light-level surrounding conditions, the sample colors of MCC (RGBCMY colors) are used as inputs of CIECAM02 with the parameters of dark surroundings. Similarly, the sample colors of MCC of the reference image are used as inputs of CIECAM02 with

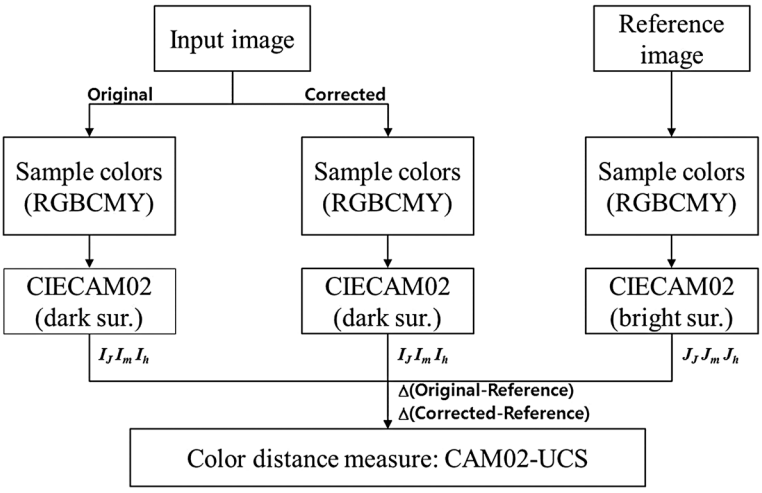

Fig. 6 Flowchart of the evaluation method using CIECAM02

Table 1 Input parameters for the CIECAM02 model

Viewing condition	Parameters of surroundings		
	C	N_c	F
Dark	0.525	0.8	0.8
Dim	0.59	0.9	0.9
Average(bright)	0.69	1.0	1.0

parameters of bright surroundings, since it is captured by the same camera under bright surrounding conditions (100 lx). The surroundings parameters for CIECAM02 are shown in Table 1 [4]. CAM02-UCS (uniform color space) is also utilized to measure the color difference [19]:

$$\Delta E_{CAM02-UCS} = \frac{1}{N}\sum_{n\in N}\left(\left\{\left[\Delta_{\overline{J'}(n)}\right]/k_L\right\}^2 + \left[\Delta_{\overline{a'}(n)}\right]^2 + \left[\Delta_{\overline{b'}(n)}\right]^2\right)^{1/2}, \tag{23}$$

where $\Delta\overline{J'} = \overline{I}_{J'} - \overline{J}_{J'}$ $\Delta\overline{J'} = \overline{I}_{J'} - \overline{J}_{J'}$, $\Delta\overline{a'} = \overline{I}_{a'} - \overline{J}_{a'}a$, $\Delta\overline{b'} = \overline{I}_{b'} - \overline{J}_{b'}$, $I_{J'} = \frac{(1+100c_1)I_J}{1+c_1 I_J}$, $I_{a'} = I_{M'}cos(I_h)$, $I_{b'} = I_{M'}sin(I_h)$, and $I_{M'} = (1/c_2)ln(1 + c_2 I_M)$ [19]. I_J, I_M, and I_h are the outputs of CIECAM02 as shown in Fig. 6. The k_L, c_1, and c_2 coefficients for the CAM02-UCS are 1.00, 0.007, and 0.0228, respectively

Table 2 shows a significant improvement of the corrected image in terms of the color reconstruction quality. The original images were under three different lighting levels (6, 9, and 12 lx). We tested the color correction performance under four color-space. Experimental result shows that the proposed method has improvement in performance over at least 4.7 to 37.1 %. The quantitative evaluation results obtained under three lighting condition are averaged. We confirmed that our method reduced the errors of the corrected images.

4.3 Color reproduction analysis

From a color reproduction perspective [20], the proposed method also enlarges an image gamut. Figure 7 shows the results on the *xy* chromaticity diagram and *ab* plane of the CIEL

Table 2 The quantitative evaluation result

Evaluation	Error		Improvement
	Original	Corrected	
ΔE_{xyz}	0.098	0.086	12.5 %
ΔE_{ab}	37.43	33.79	9.7 %
ΔE_{00}	6.19	3.89	37.1 %
$\Delta E_{CAM02-UCS}$	59.90	57.11	4.7 %

Improvement (%) = $(E_{original} - E_{correct})/E_{original}$

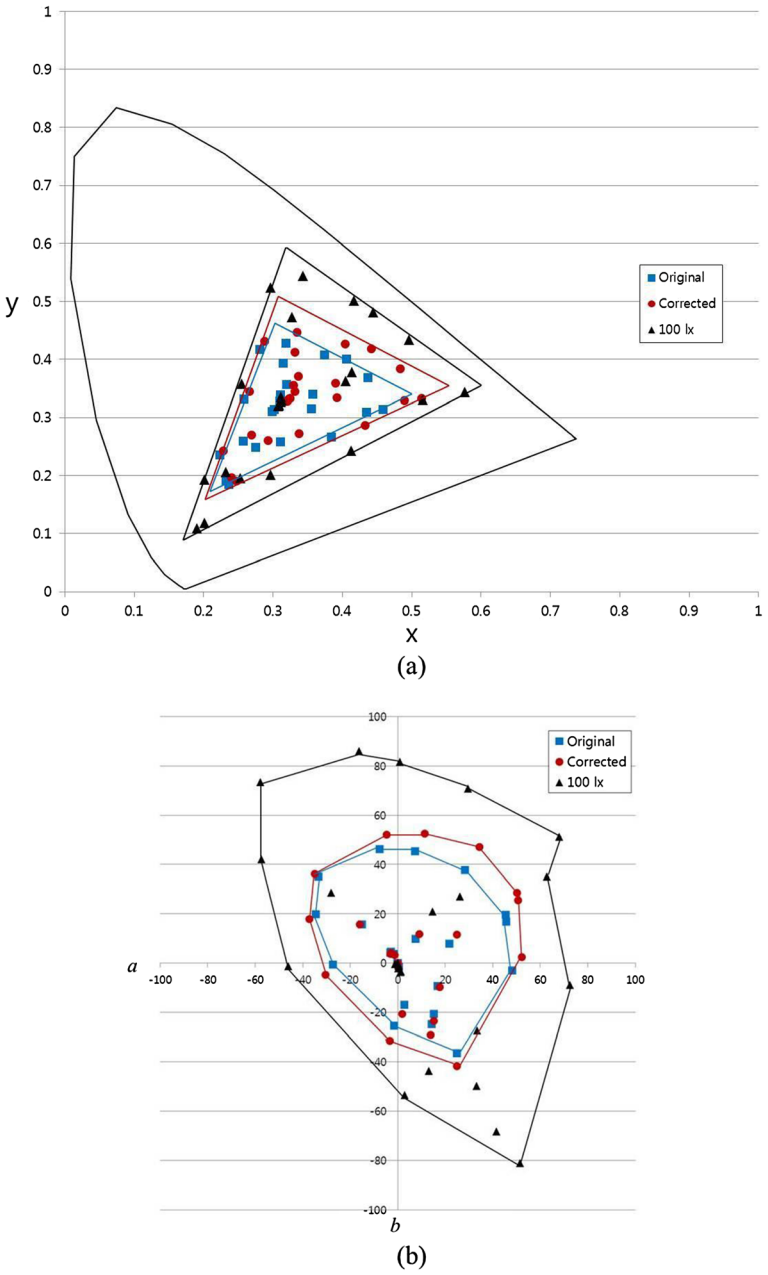

Fig. 7 Color reproduction results: **a** *xy* chromaticity diagram and **b** *ab* plane

AB. The horseshoe-shaped curve of Fig. 7a indicates the range of the HVS. We could find that the corrected images have a wider distribution than the original images, indicating that the EMCCD camera with the color correction can express more various ranges of colors. In

summary, Y and Z values are corrected by our proposed method, and X value is almost the same as described below:

$$\begin{cases} x^{(\uparrow\uparrow)} = \dfrac{X}{X + Y^{(\downarrow)} + Z^{(\downarrow\downarrow)}} \\ y^{(\uparrow)} = \dfrac{Y^{(\downarrow)}}{X + Y^{(\downarrow)} + Z^{(\downarrow\downarrow)}}\ a \\ z^{(-)} = \dfrac{Z^{(\downarrow\downarrow)}}{X + Y^{(\downarrow)} + Z^{(\downarrow\downarrow)}}, \end{cases} \tag{24}$$

where XYZ are components on CIEXYZ color space, and superscripts in bracket represent the increase or decrease amount of expressive range. Thus, we can conclude that our method effectively corrects the original color image obtained from the EMCCD camera, resulting in vivid colors and an enlarged expressive color range similar to the reference image. Figure 7b also shows the strength of our method. Specifically, a relative ratio of the area between the reference and corrected images is 42 %, while that of the original images is 32 %.

5 Conclusion

In this paper, we proposed the SSF correction method for an EMCCD camera. The SSF measured from the EMCCD camera demonstrates that the EMCCD camera sensor characteristics are partially uni-modal, positive, and reasonably smooth. We correct output colors of the EMCCD images by removing the secondary response of bi-modal SSFs in some channels (here, G and B channels). In addition, our method has some advantages, including the quality improvement from the color appearance perspective and the enlargement of the gamut. We plan to devise various practical low-light-level applications based on this correction method.

Acknowledgments This work was supported by the National Research Foundation of Korea (NRF) grant funded by the Korea government (MSIP) (NRF-2013R1A2A2A01068338).

References

1. Barnard K, Funt B (2002) Camera characterization for color research. Color Res Appl 27(3):152–163
2. Coates C, Denvir D, McHale N, Thornbury K, Hollywood M (2003) Ultra-sensitivity, speed and resolution: optimizing low-light microscopy with the back-illuminated electron multiplying CCD. Proc SPIE 5139:56–66
3. Denvir D, Conroy E (2003) Electron multiplying CCD technology: the new ICCD. Proc SPIE 4796:167–174
4. Fairchild M (2005) Color appearance models, 2nd edn. Addison-Wesley, Reading
5. Finlayson G, Hordley S (2001) Color constancy at a pixel. J Opt Soc Am A 18(2):253–264
6. Finlayson G, Hordley S, Lu C, Drew M (2006) On the removal of shadows from images. IEEE Trans Pattern Anal Mach Intell 28(1):59–68
7. Finlayson G, Hordley S, Hubel P (1998) Recovering device sensitivities with quadratic programming. In: Proceedings of the IS&T/SID 6th color imaging conference: color science, systems and applications, Scottsdale, Arizona, Nov 1998, pp 90–95
8. Francisco G, Roberts S (2004) Security surveillance challenges and proven thermal imaging capabilities in real-world applications, defense and security. Int Soc Opt Photonics: 811–822
9. Holst G, Lomheim T (2007) CMOS/CCD sensors and camera systems. SPIE Press, Bellingham
10. Hong G, Luo M, Rhodes P (2001) A study of digital camera colorimetric characterization based on polynomial modeling. Color Res Appl 26(1):76–84

11. Jerram P, Pool P, Bell R, Burt D, Bowring S, Spencer S (2001) The LLLCCD: low light imaging without the need for an intensifier. Proc SPIE 4306:178–186
12. Jerram P, Pool P, Burt D, Bell R, Robbins M (2006) Electron multiplying CCDs, in SNIC symposium: 1–5
13. Johnson C (1998) Review of electron-bombarded CCD cameras. Proc SPIE 3434:45–53
14. Kang H, Anderson P (1992) Neural network applications to the color scanner and printer calibrations. J Electron Imaging 1(2):125–134
15. Kang M, Kim B, Sohn K (2009) CIECAM02-based tone mapping technique for color image contrast enhancement. Opt Eng 48(8), 087001
16. Kang M, Yang U, Sohn K (2011) Spectral sensitivity estimation for EMCCD camera. IET Electron Lett 47(25):1369–1370
17. Kriesel J, Gat N (2006) Performance tests of true color night vision cameras. In: Military Sensing Symposia(MSS) specialty group on passive sensors, Orlando, FL, Feb 2006
18. Kriesel J, Gat N (2010) True-color night vision (TCNV) fusion system using a VNIR EMCCD and a LWIR microbolometer camera. Proc SPIE 7697, 76970Z 1–8
19. Luo M, Cui G, Li C (2006) Uniform colour spaces based on CIECAM02 colour appearance model. Color Res Appl 31(4):320–330
20. Morovic J, Luo M (2001) Evaluating gamut mapping algorithms for universal applicability. Color Res Appl 26(1):85–102
21. Robbins M, Hadwen B (2003) The noise performance of electron multiplying charge-coupled devices. IEEE Trans Electron Devices 50(5):1227–1232
22. Sharma G, Trussel H (1993) Characterization of scanner sensitivity. In: Proceedings of the IS&T/SID color imaging conference: transforms and portability of color, 103–107
23. Sharma G, Wu W, Dalal E (2005) The CIEDE2000 color difference formula: implementation notes, supplementary test data, and mathematical observations. Color Res Appl 30(1):21–30
24. Shen H, Xin J (2004) Spectral characterization of a color scanner by adaptive estimation. J Opt Soc Am A 21(7):1125–1130
25. Zhang W, Dai D (2008) Spectral reflectance estimation from camera responses by support vector regression and a composite model. J Opt Soc Am A 25(9):2286–2296

Jongin Son received the B.S. degree in electronic engineering from Korea Polytechnic University, Korea, in 2008. He is currently pursuing the joint M.S. and Ph.D. degrees in electrical and electronic engineering in Yonsei University, Seoul, Korea. His research interests include color image processing, human visual system, and intelligent vehicle system.

Minsung Kang received the B.S. and joint M.S./Ph.D. degrees in electronic and electrical engineering from Yonsei University, Seoul, Korea, in 2006 and 2014. He is currently a senior research engineer in LG Display, Korea. His research interests include color image processing, human visual system, and image quality assessment.

Dongbo Min received the B.S., M.S., and Ph.D. degrees from the School of Electrical and Electronic Engineering, Yonsei University, in 2003, 2005, and 2009, respectively. From 2009 to 2010, he was with Mitsubishi Electric Research Laboratories as a Post-Doctoral Researcher, where he developed a prototype of 3D video system. From 2010 to 2015, he was with the Advanced Digital Sciences Center, Singapore, which was jointly founded by the University of Illinois at Urbana-Champaign and the Agency for Science, Technology and Research, a Singapore Government Agency. Since 2015, he has been an Assistant Professor with the Department of Computer Science and Engineering, Chungnam National University, Daejeon, Korea. His research interests include computer vision, 2D/3D video processing, computational photography, augmented reality, and continuous/discrete optimization.

Kwanghoon Sohn received the B.E. degree in electronic engineering from Yonsei University, Seoul, Korea, in 1983, the M.S.E.E. degree in electrical engineering from the University of Minnesota, Minneapolis, MN, USA, in 1985, and the Ph.D. degree in electrical and computer engineering from North Carolina State University, Raleigh, NC, USA, in 1992. He was a Senior Member of the Research Staff with the Satellite Communication Division, Electronics and Telecommunications Research Institute, Daejeon, Korea, from 1992 to 1993, and a Post-Doctoral Fellow with the MRI Center, Medical School of Georgetown University, Washington, DC, USA, in 1994. He was a Visiting Professor with Nanyang Technological University, Singapore, from 2002 to 2003. He is currently a Professor with the School of Electrical and Electronic Engineering, Yonsei University. His research interests include 3D image processing, computer vision, and image communication. He is senior member of IEEE and member of SPIE.